ELSEVIER

Contents lists available at ScienceDirect

## Journal of Alloys and Compounds

journal homepage: www.elsevier.com/locate/jalcom





# Novel insights into the distinct magnetic configurations of polycrystalline Ni nanowires produced by a template approach at varying electrodeposition potentials

Melania Onea <sup>a,b</sup>, Nicusor Iacob <sup>a</sup>, Gabriel Schinteie <sup>a</sup>, Maria Eugenia Toimil Molares <sup>c</sup>, Elena Matei <sup>a,\*</sup>, Victor Kuncser <sup>a,\*</sup>, Ionut Enculescu <sup>a,\*</sup>

#### ARTICLE INFO

Keywords: Electrodeposition Ni nanowires Magnetic anisotropy

#### ABSTRACT

Electrochemical replication of nanoporous membranes was employed for the fabrication of nickel nanowires. The fabrication process led to uniform arrays of quasi 1 dimensional nanoobjects with low diameters and high aspect ratios. Extensive characterization experiments were carried out for determining the morphological, structural and magnetic properties of the nanostructures. It was found that the working electrode potential employed during the electrochemical deposition fabrication experiments influences both the crystalline structure and the magnetic properties of the nanowires. Accordingly, an in-depth investigation of the correlations between the morpho-structural and the magnetic parameters was performed. It was shown that several structural factors, mainly crystalline texture and grain size and shape, quite sensitive to the deposition potential, influence also the specific magnetic configurations, which can be tuned from 3-dimensional Imry and Ma random anisotropy type to cooperative quasi-1-dimensional superspin type. Consequently, new possibilities in tailoring the magneto-functionalities of polycrystalline magnetic nanowires by adjusting fabrication parameters are revealed.

### 1. Introduction

Due to the continuous search for the development of new electronic devices which shall exploit specific magnetic properties of nanostructures, especially in connection with related magneto-resistance effects new cost-efficient methods for their controlled fabrication are of high interest. Various engineering approaches employed for tailoring specific functionalities of magnetic nanostructures of reduced dimensionality are being sought and tested. Magnetic nanowires and magnetic nanotubes are considered a particular class of such nanoobjects which can be used in a wide range of applications including magnetoresistive sensors, data storage elements and information processing spintronic devices. Their magnetic properties are controlled by morphology (aspect ratio and specific sizes), composition and crystalline structure, and can be easily tuned, making them perfect candidates for such novel devices. Previous studies on arrays of Ni-Cu magnetic nanowires, for which the magnetic properties are tuned via the alloy composition and interelements magnetic interactions as well as on Ni/NiO concentric

nanotubes with dominant unidirectional anisotropy at the ferromagnetic/antiferromagnetic interface have been reported [1,2].

Numerous experimental methods have been described for the controlled fabrication of magnetic nanowires including lithographical techniques, chemical vapor deposition and hydrothermal growth [3–5]. The main purpose of all these specific methods is to have a good control of morphology, structure and composition simultaneously, in order to succeed in tailoring the magnetic properties of the nanowires.

A very useful technique to fabricate nanowire arrays is electrochemical deposition inside nanoporous membranes [6-10]. Some of the advantages of this method are low cost, high reproducibility and low temperature fabrication. By using this approach to obtain nanowires, one can control both their morphology (by means of the template) and their composition (by means of electrolyte end deposition conditions). Consequently, the magnetic properties of such nanowires can be tuned in agreement with the foreseen applications. The templates used for fabricating nanowires are usually nanoporous ion track polycarbonate membranes [11-15] and anodic alumina membranes [16].

E-mail addresses: elena.matei@infim.ro (E. Matei), kuncser@infim.ro (V. Kuncser), encu@infim.ro (I. Enculescu).

<sup>&</sup>lt;sup>a</sup> National Institute of Materials Physics, Atomistilor 405A, Magurele, Ilfov 077125, Romania

<sup>&</sup>lt;sup>b</sup> Faculty of Physics, University of Bucharest, Atomistilor 405, Magurele, Ilfov 077125, Romania

<sup>&</sup>lt;sup>c</sup> GSI Helmholtzzentrum für Schwerionenforschung GmbH, Planckstraße 1, Darmstadt 64291, Germany

<sup>\*</sup> Corresponding authors.

Rhombohedral Ni and Ni-B nanotubes have been grown by electroless-plating in track-etched mica templates [17] whereas hexagonal arrays (lattice parameters ranging from 65 to 105 nm) of Ni nanowires with different diameters (18–83 nm) have been prepared by filling self-ordered nanopores in alumina templates [18].

In this paper an investigation on the magnetic properties of Ni nanowires fabricated by means of a template electrochemical replication route, using as templates nanoporous ion track polycarbonate membranes irradiated with swift heavy ions, is reported. The aim is to prove the experimental possibility to tune the magnetic anisotropy of the wires by suitable choosing the electrodeposition potentials. The complexity of the obtained magnetic configurations is discussed, showing the role of the structural texture on the interplay between the different components of anisotropy. The report delivers a comprehensive correlation between the magnetic properties and the morphostructural features resulting from the preparation conditions. It is shown that not only the typical geometric parameters responsible for the magnetostatic energy (shape anisotropy) or dipolar interactions among the nanowires are essential for the involved magnetic anisotropies, as usually reported (see for example [19] and [20]) but also the local structural aspects accountable for the specific magnetic configuration inside the nanowires.

#### 2. Experimental details

The Ni nanowires were prepared using the template-assisted electrodeposition technique. The templates used were nanoporous polycarbonate membranes having a thickness of 30 micrometres, a density of  $10^8$  pores/cm² and a pore diameter of about 100 nm. Swift heavy ions of approximately 10 MeV/nucleon (irradiation was performed at GSI Unilac) were used for producing the ion tracks with the desired surface density. The chemical etching/removal of the ion tracks was made by immersing the membranes in an aqueous solution of 5 M NaOH and 10 % vol. methanol at a temperature of  $50^{\circ}$ C. The working electrode, a thin film (50 nm) of Au, was deposited by sputtering on the back of the polycarbonate membrane and was subsequently thickened electrochemically with a layer of Cu ( $10 \mu m$ ).

Electrochemical deposition was performed using a potentiostat galvanostat (PARSTAT 2276) controlled by a PC employing a typical configuration of three electrodes: a platinum foil of 1 cm $^2$  (counter electrode), the thin film of Au (working electrode) and a saturated calomel electrode (SCE) as a reference electrode. The temperature used during deposition (50°C) was kept constant by employing a double wall electrochemical cell and a recirculating bath. The nanowires were obtained at four different working electrode potentials: -700, -800, -900 and -1000 mV measured versus the reference electrode, leading to sample codes S1, S2, S3 and S4, respectively. The aim was to investigate the influence of the electrodeposition potential on the magnetic properties of the nanowires.

The morphology and composition of the wires were analyzed by scanning electron microscopy (SEM) and energy dispersive X ray spectroscopy (EDX), after dissolving the membranes in dichloromethane. A field emission scanning electron microscope (Zeiss, Gemini 600) with a Bruker EDX accessory was employed for this specific set of experiments.

X-ray diffraction (XRD) investigations have been performed in order to assess the structure of the nanowire arrays, including here the dominant growth direction (texture) resulting from the specific experimental conditions. For structural analysis a Brucker D8 Advance diffractometer with Cu  $K_{\alpha}$  radiation was employed. An alternative parametrization of the crystalline texture based on the consideration of peak intensities in the XRD patterns, according to [21], has been considered. The lattice parameter, based on the diffraction peak positions and grain size and stain parameters, based on the full width at half intensity (FWHM) of the diffraction peaks have been estimated according to [22]. The gaussian (for grain size estimation) and Lorentzian (for strain estimation) components of FWHM were obtained by fitting

the experimental peaks by Voight profiles, according to [23].

The magnetic measurements have been performed by SQUID magnetometry (MPMS XL magnetometer from Quantum Design) under the high sensitivity reciprocal space option, RSO (4 cm of sample movement, linear regression mode). Identical samples consisting of disks of 3 mm diameter (0.070(2) cm<sup>2</sup> area, with the number in brackets meaning the error at the last-mentioned digit) were cut from the polycarbonate template with Ni nanowires via an eyelet. The nanowires grown inside the etched tracks are perpendicular on the template (the fact that the wires are parallel with a very narrow angular distribution of less than  $5^{\circ}$  with respect to the normal direction is to be mentioned). Magnetic hysteresis loops were collected at different temperatures on the considered samples. The magnetic field was applied both perpendicular to the foil (i.e. with the field along the wires, giving rise to the configuration called parallel) and along the foil plane (with the field perpendicular to the wires, giving rise to the configuration called perpendicular). The saturation magnetization in different geometries and at different temperatures were computed according to the low of approach to saturation based on the extrapolation of magnetization in high fields versus the inverse of the magnetic field [24]. In this respect, the hysteresis loops in different geometries were acquired in corresponding high enough fields.

#### 3. Results and discussion

SEM images of arrays of nanowires deposited at -700 and -1000 mV are shown in Fig. 1 (lower magnification arrays of nanowires, left hand and detail of single nanowire, right hand).

The SEM images confirm that the growth process took place as expected, with the wires growing as replicas of the pores' arrays. The average distance between neighboring wires is as expected from the considered pore density, while the average diameter of the wires is of approximately 100 nm, with a relatively low size dispersion. SEM investigations after the chemical etching of the template proves the formation of continuous wires in lengths of about 30  $\mu m$  (the number of broken wires during the growing process, due to voids formation, is negligible in all samples).

The XRD patterns collected from measurements performed on samples obtained under different electrodeposition potentials (as well as on a control sample) are shown in Fig. 2. The evolution of the lattice parameter versus the deposition potential is shown in the inset. It can be observed at a glance that the typical fcc structure of Ni is obtained as well as the fact that the average lattice parameter is almost constant with the deposition potential. The lattice parameter in all investigated samples (calculated via the Nelson-Riley dependence of the positions of the 3 main diffraction peaks of Ni in Fig. 2 [A2] equates the value of 3.5195(5) nm, i.e. a less than 0.3 % lower than the bulk value of well crystallized Ni reported in literature (3.5295 nm) [14], according to JCPDS 04–850. Consequently, the density of the metallic Ni forming the nanowires is independent on the deposition potential and is almost similar to the density of the bulk metallic Ni.

Magnetic hysteresis loops collected at different temperatures on the mentioned samples consisting of cylindrical magnetic nanowires in polycarbonate templates, in two geometries are presented in Fig. 3. Here para means parallel geometry, indicating the applied magnetic field parallel to the nanowire axis and perp means perpendicular geometry, indicating the applied magnetic field perpendicular to the nanowire axis. The magnetization is reported in emu per gram of magnetic material (metallic Ni in this case). The amount of Ni in each sample was computed by multiplying the volume of the magnetic material by the theoretical density of metallic Ni (8.9 g/cm³), according to the above observation related to the value of the lattice parameter in the samples. The volume of the magnetic material was estimated by considering the surface of the disk-like sample (0.070 cm²), the surface wire density equating the pore density ( $10^8 \ \text{cm}^{-2}$ ), the average length of the wire equating the thickness of the polycarbonate membrane (0.003 cm) and

Fig. 1. SEM images: (a) Array of nanowires deposited at -1000 mV; (b), (c) Detail of a nanowire deposited at -1000 mV and -700 mV, respectively.

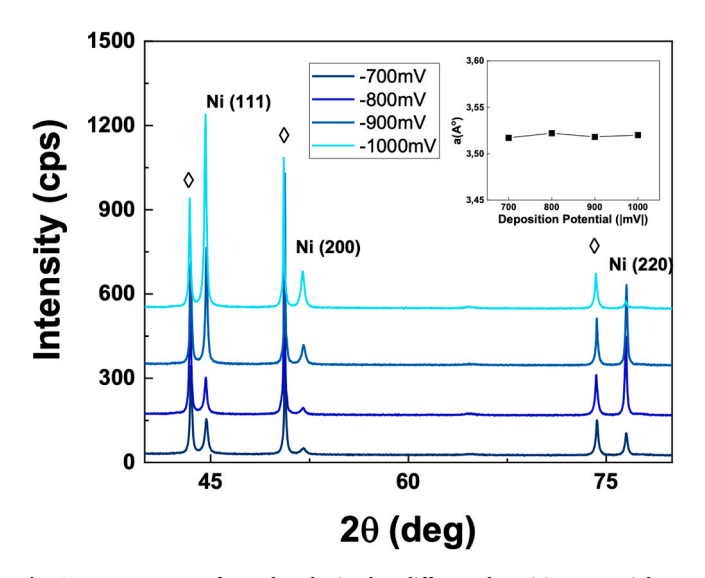


**Fig. 2.** XRD patterns of samples obtained at different deposition potentials. In diamond symbols are marked the peaks corresponding to the same reflection planes as for Ni, but belonging to the thickening Cu layer. The evolution of the lattice parameter of metallic Ni versus the deposition potential is shown in the inset.

the wire average diameter  $(10^{-5}~\text{cm})$ , all these quantities being estimated with a relative error of a few percent. Accordingly, the average volume of the magnetic material in each sample is  $1.66\cdot 10^{-6}~\text{cm}^3$ , whereas the average amount of magnetic material is  $1.48\cdot 10^{-5}~\text{g}$ , also with a relative error of a few percent.

All the above assumptions are strongly supported by the available imagistic on each sample, taken at different stages (as prepared, after dissolving the polymer and after dispersing the wires). Also, a very low amount of unfilled/not completely filled pores (less than 1 %) have to be mentioned. By following typical methodological tools, the deposition was stopped after reaching the maximum current, i.e. at the moment of a complete filling of the pores. A quite similar charge exchanged through the working electrode was obtained by integrating the current during the pore filling for each sample, supporting a similar amount of deposited magnetic material in the pores for all samples.

Some observations are directly resulting from Fig. 3. Except the difference in the shape of the hysteresis loops collected in the two geometries which will be discussed in the following, an unexpected difference in the saturation magnetization obtained in the two measurement geometries at similar temperature must be noted (e.g. in case of sample obtained at the eletrodeposition potential of  $-700 \, \mathrm{mV}$ , the saturation magnetization at 300 K is 33 emu/g in parallel geometry and 40 emu/g in perpendicular geometry). This has to be due to some artifacts and possible pitfalls of the SQUID magnetometer, unfortunately quite rarely discussed in literature [25,26].

Accordingly, in [25] the deviations of the magnetic flux in the collecting gradiometer pickup coil relative to a point dipole sample are computed for different geometrical distributions of the magnetic moment. In case of a sample with a magnetic moment of about  $10^{-3}\,\mathrm{emu}$ 

(close to the value of the investigated samples measured under the linear regression mode) distributed in the sample plane, a deviation of -21.55 % is reported for a geometry with the magnetic field perpendicular to the sample plane (para- in the present notation) and of only -1.98 % for a geometry with the magnetic field parallel to the sample plane (perp-in the present notation). Evidently, it is this perp geometry (with the magnetic field applied perpendicular to the nanowires) which provides the most reliable value of the specific magnetization from the saturation magnetization. Although a progressive saturation is observed for these samples at 5 K under an applied magnetic field of 20 kOe, making somehow more difficult a precise estimation of the saturation magnetization at low temperature, the saturation is complete at 300 K. Saturation magnetizations decreasing with the deposition potential from about 40 emu/g in sample S1 down to about 20 emu/g in sample S4 are obtained at 300 K. For sure, a such decrease of magnetization by 50 % among samples S1 and S4 cannot be explained by an expected few percent variation in the mass of the magnetic material among the 2 samples, as previously discussed. While the reported value of specific magnetization for metallic Ni at room temperature is 55.09 emu/g, two additional questions are raising up: (i) the reason for such a low saturation magnetization of the analyzed samples proven to consist of well crystallized metallic Ni with a lattice parameter only 0.3 % lower than the bulk value and (ii) the reason for the strong decrease of the saturation magnetization of samples obtained at higher deposition potentials, in case of similar structure and lattice parameters of the analyzed samples. As will be seen in the following, the answer is provided by the specific magnetic structure strongly depending on the deposition potential, which also explains the specificities of the hysteresis loops in the

Concerning the geometry dependent hysteresis loops, they change from a more rounded shape in parallel geometry to an almost linear shape followed by progressive saturation in the perpendicular geometry, with specific magnetic parameters depending on both temperature and preparation conditions. This general geometry dependent behavior is specific to cylindrical magnetic nanowires where the magnetization reversal mechanism was extensively reported [2,27–29]. To note at this point that in case of the sample obtained at the lowest deposition potential (hereafter we will refer always to its magnitude), the hysteresis loop collected in parallel geometry at the lowest temperature, where dynamical magnetic effects are negligible, evidences an additional less intense magnetic component of higher coercive field which superposes over the main component characterized by a slightly lower coercive field. This effect should be related to some structural inhomogeneity in this sample which will be neglected in a first approximation, especially if the main hysteretic component will be taken into consideration in the further discussion.

For the investigated array of nanowires, the reversal mechanism depends on both the reversal mechanism of individual nanowires as well as on the dipolar interactions among the nanowires. Arrays of Ni-Cu nanowires with up to 92 % of Ni, 90 nm in diameter and embedded in 30  $\mu$ m thick polycarbonate membranes ( $10^9$  cm<sup>-2</sup> density area) were reported in [2], showing a similar geometry dependent behavior. Negligible dipolar interactions among wires are estimated by the simplified expression provided by [30]:  $E_{\rm int} = \Phi_i \Phi_j / Rn$ , where  $R_n$  is the average distance between two neighboring nanowires and  $\Phi_i$ 

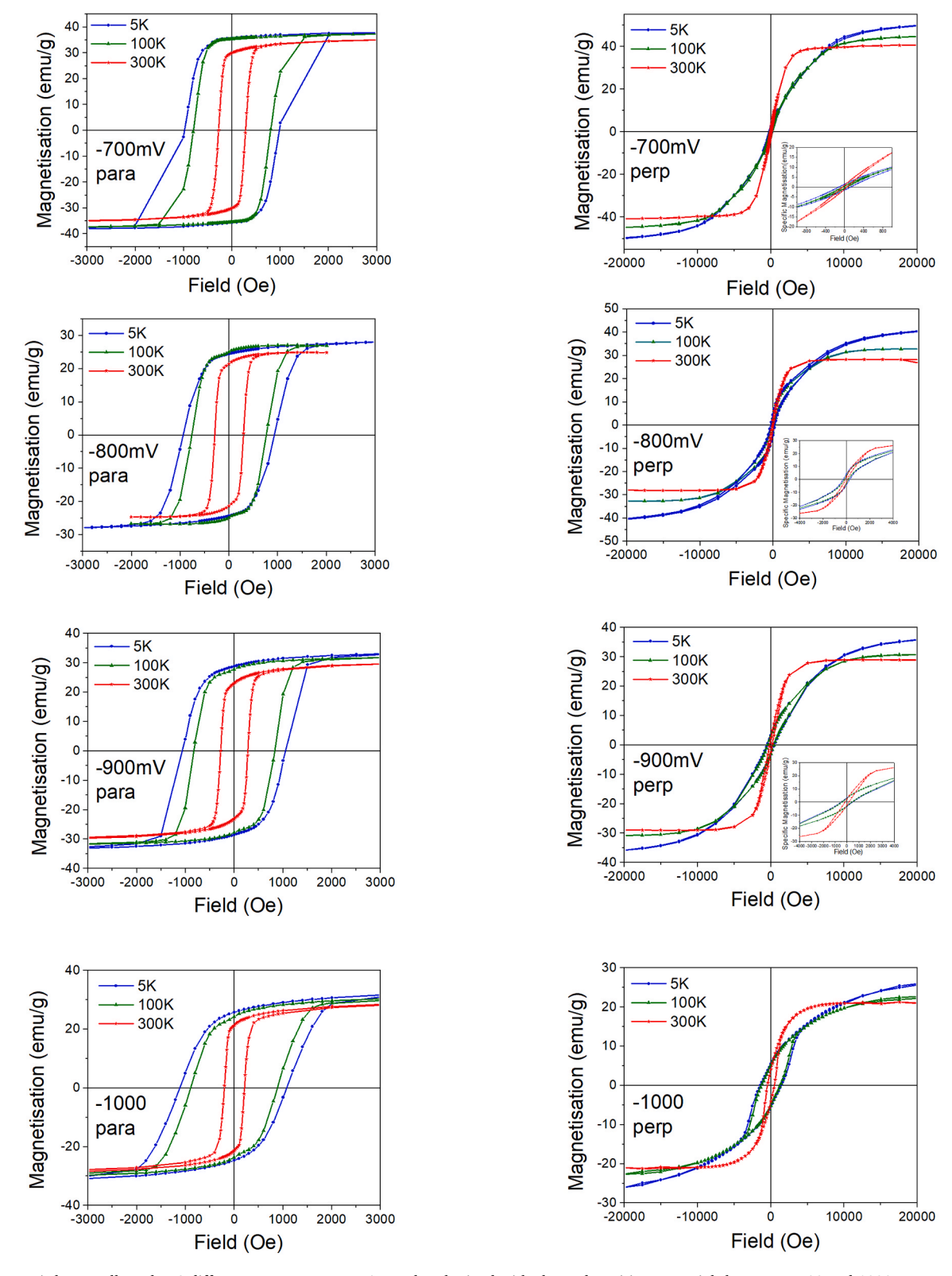


Fig. 3. Hysteresis loops collected at 3 different temperatures on 4 samples obtained with electrodeposition potentials between -700 and-1000 mV. Two measuring geometries are considered: para –with the magnetic field applied along the nanowires (left side) and perp-with the magnetic field applied perpendicularly to the nanowires (right side).

 $\alpha_i \pi M_i D^2/4$  with  $\alpha_i = \pm 1$ , D the wire diameter and  $M_i$  the magnetization of entity i (about 58 emu/g or  $5^*10^5$  A/m for metallic Ni [31]). Roughly, an average field lower than 0.5 Oe is required to destroy the antiferromagnetic interaction between two neighboring nanowires, which is also in line with the estimation reported in [2] for the case of nanowires with

92 % of Ni approaching closely the case of pure Ni nanowires, given the fact that one order of magnitude lower pore density is considered in the present study. While saturation and coercive fields approaching 1000 Oe are implied in parallel geometry at low temperature in the present situation, the magnetization reversal mechanism of the

investigated array of nanowires must be clearly related to the reversal mechanism of individual nanowires.

The magnetization reversal in individual nanowires has been studied for long time. Both the aspect ratio and the wire diameter influence the magnetic domain structure, especially when the diameter is related to the exchange length parameter  $\lambda_{ex} \approx \sqrt{A/K}$  with K the anisotropy constant and A the stiffness constant. In case of cylindrical Ni nanowires of high aspect ratio, the dominant anisotropy energy is the shape anisotropy. Consequently, K can be approximated by the formula  $K \approx \pi M_s^2$  [32]. By taking  $M_S$  as about  $5*10^5$  A/m and A as about  $9*10^{-12}$ J/m [31,33], it was shown that for Ni nanowires there is threshold diameter of about 12 nm, below which a coherent magnetization reversal takes place. Above this size a curling mode reversal is induced by a field applied along the cylinder length. In fact, the curling mode involves the nucleation and subsequent propagation of thin domain walls at the 2 ends of the nanowires with different spin rotations in the domain. It was shown in [32] that 2 modes can be induced depending on the wire diameter in these conditions, namely a transverse wall mode (the magnetization remains homogeneous through any radial cross section of the cylinder), if the diameter is lower than a critical diameter  $d_c$  about 40 nm in case of Ni nanowires, and the vortex wall mode (a vortex structure of magnetization in the radial cross section) at diameters larger than  $d_c$ . The dynamics of the domain walls involving both nucleation and domain wall propagation was studied in [34], showing that the magnetization reversal in Ni nanowires of 40 nm in diameter and micron range length takes place in nanosecond time range leading to a similar but inverted magnetic domain structure before and after magnetization reversal (e.g. all spins are oriented along the cylinder axis which is the easy axis of magnetization). By contrary, a coherent progressive magnetization reversal takes place if the field is applied perpendicular to the cylinder length with the saturation field respecting the Stoner-Wohlfarth switching field, H<sub>SW</sub>, always larger than the switching field through domain wall propagation. Hence, a rectangular hysteresis loop is obtained in longitudinal geometry and a linear one in perpendicular geometry, with the saturation field in perpendicular geometry higher than the switching field (equating the coercive field of the rectangular loop) in longitudinal/parallel geometry. It is that saturation field in perpendicular geometry where a coherent rotation takes place, which equates  $H_{SW}=2K/M_S$  and can be compared with the experimental values. In the present case, a shape anisotropy can be considered as dominant and as consequence, the anisotropy constant can be evaluated according to the formula  $K \approx \pi M_s^2$ .  $M_s$  at low temperature, as evaluated from the hysteresis loops in perpendicular geometry presented in Fig. 3., is about 46 emu/g (409 emu/cm<sup>3</sup>) for sample S1, 36 emu/g (320 emu/cm<sup>3</sup>) for samples S2 and S3 and 24 emu/g (214 emu/cm<sup>3</sup>) for sample S4. Hence, shape anisotropy constants of about 5.2\*10<sup>5</sup> erg/cm<sup>3</sup>  $(5.2*10^4 \text{ J/m}^3)$ ,  $4.1*10^5 \text{ erg/cm}^3 (4.1*10^4 \text{ J/m}^3)$  and  $2.7*10^5 \text{ erg/cm}^3$  $(2.7*10^4 \text{ J/m}^3)$  are obtained for the above samples, respectively. Having in mind that the cubic magneto-crystalline anisotropy of face centered cubic Ni is defined by  $^{25}$   $K_1 = -5*10^3$  J/m<sup>3</sup> and  $K_2 = 2*10^3$  J/m<sup>3</sup>, it is clear that the shape anisotropy strongly dominates over the magneto-crystalline one. Therefore, an overall uniaxial anisotropy with the easy axis of magnetization along the cylinder length is also expected for the investigated samples.

Micromagnetic calculations on high aspect ratio single Ni-Cu nanowires with diameters of 100 nm (similar to this case),under hypothesis of specific magnetizations ranging from  $6.2 \cdot 10^5$  A/m (69 emu/g) down to  $3.1 \cdot 10^5$  A/m (34 emu/g) and stiffness constants ranging from  $7 \cdot 10^{-12}$  J/m down to  $3.5 \cdot 10^{-12}$  J/m have been reported in [1]. Notably, the simulation is valid for any magnetic system with the above mentioned parameters, independently on the physical reason leading to their variation (e.g. pure Ni nanowires with specific morpho-structural aspects leading to noncolinear spin structure and hence with decreased specific magnetization or with magnetic defects decreasing the stiffness constant). The same specific change of the hysteresis loop

from a rectangular shape, with the field applied along the nanowire, to a linear shape, with the field applied perpendicular to the nanowire, and saturation fields much higher in perpendicular geometry than in parallel geometry is reported. For similar magnetic parameters (saturation magnetization and shape anisotropy constant) to the ones of samples S2 and S3, the calculated linear loop in perpendicular geometry is characterized by a sharp saturation reached around a saturation field of only 1900 Oe. By contrary, in the investigated samples a quite progressive saturation which is not complete even in fields higher than 10.000 Oe takes place. It should be noted that a quasi-saturation field is experimentally approached by using the tangent method, at 9000(900) Oe (in bracket is the error) for all samples from S4 to S1, increasing much slower than linearly with the magnetization, as would be expected from the simplest Stoner-Wohlfarth type coherent rotation ( $H_S = 2\pi M_S$ ). This is a first hint that local magnetic defects are present in the samples, which on one hand introduce additional pining effects and on the other hand may change the magnetic spin configuration in the nanowire. As expected, saturation magnetizations lower than in theory can be assigned to non-collinear magnetic configurations. Such configurations deviate from the ferromagnetic linear ones where the spins are parallel to nanowire length and can be due to distributed local anisotropies axes leading for example to flower-like spin structures maintained also under higher fields. According to the experimentally obtained different saturation magnetization values obtained for the 4 samples, a different magnetic texture depending on the deposition potential would be also expected for these samples. To note that the spin texture can be characterized in average by an angular spin distribution with a symmetry axis along the cylinder axis (also representing the easy axis of magnetization in the present case). However, except this average characterization of the magnetic texture, a spatial distribution of the spin orientations can be present, in close relation to the crystallite shape and orientations and hence of the crystalline texture.

Concerning the magnetic texture of a nanowires array, reduced in the present case to the average magnetic texture of independent nanowires, it can be easier characterized via the above exposed reasoning by the ratio R = M<sub>R</sub>/M<sub>S</sub> obtained in the two geometries (perpendicular and parallel to the nanowire). For unidirectional orientations of the spins (complete texture) the ratio  $R_{\text{perp}}$  in perpendicular geometry should be 0 whereas in parallel geometry,  $R_{\text{para}}$  should be 1. In case of a lower texture R<sub>perp</sub> increases from 0 whereas R<sub>para</sub> decreases from 1, both ratios taking the value of 0.5 in case of randomly oriented magnetic moments (no magnetic texture). Consequently, the ratio R<sub>para</sub>/R<sub>perp</sub> takes a very high value (approaching ∞) for very high magnetic texture and 1 for no magnetic texture. The temperature evolution of the M<sub>R</sub>/Ms ratios in the two geometries for all samples S1 to S4 is shown in Fig. 4. According to Fig. 4, the most texture sensitive ratios  $R_{\text{para}}/R_{\text{perp}}$  calculated at low temperature where magnetic dynamical effects are neglected are 31, 30, 10 and 3.5 for samples S1, S2, S3 and S4, respectively. It is clearly observed from these data that the magnetic texture decreases strongly for samples obtained at more electronegative potentials until -1000 mV.

On the other hand, one may consider that the crystalline texture can be parametrized by a texture coefficient ( $T_C$ ) according to Eq. (1), by considering the most intense diffraction lines corresponding to the (111), (200) and (220) reflection planes of the fcc structure of Ni:

$$T_{C}(h_{i}k_{i}l_{i}) = \frac{I(h_{i}k_{i}l_{i}) / \sum_{i=1}^{3} I(h_{i}k_{i}l_{i})}{I_{0}(h_{i}k_{i}l_{i}) / \sum_{i=1}^{3} I_{0}(h_{i}k_{i}l_{i})},$$
(1)

where  $I(h_ik_il_i)$  is the intensity of the diffraction line corresponding to the reflection plane  $(h_ik_il_i)$  in the investigated sample, whereas  $I_0(h_ik_il_i)$  is the intensity of the diffraction line corresponding to the same reflection plane  $(h_ik_il_i)$  in a reference polycrystalline sample with no crystalline texture.

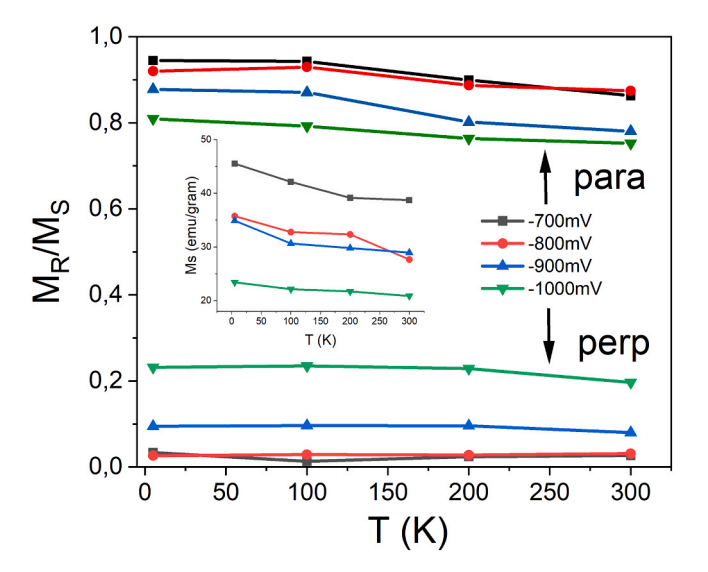


**Fig. 4.** Evolution of the  $M_R/M_S$  ratio (the ratio between the saturation magnetization,  $M_S$  and the remanent magnetization,  $M_R$ ) function of temperature, for samples obtained at different electrodeposition potentials. The same two geometries, with the field applied parallel (para) and perpendicular (perp) to the nanowires are considered. The inset shows the temperature evolution of the saturation magnetization in perpendicular geometry which gives the best estimation for the real values of saturation magnetization.

The values of  $T_C$  for the 3 mentioned reflection planes are presented in Fig. 5(a) for all the investigated samples. According to this Eq. (1),  $T_C$  values equal to 1 means random distributions of such reflection planes. Higher than 1 are the  $T_C$  values for which a higher probability to form such parallel planes along their normal direction is inferred (e.g. an increased texture for those planes). Accordingly, an increased texture for the (220) plane is to be mentioned in samples obtained for deposition potentials more electropositive than -900~mV and a sharp decrease of this possibility on the account of the increased texture along the normal to (111) planes.

Crystallite sizes and strains along the perpendicular directions to the above-mentioned reflection planes are shown in Fig. 5(b) and (c), respectively. The crystallite size in the direction perpendicular to each considered reflection plane was determined by the Sherer formula with the proportionality constant approximated to 1 and considering the gaussian component of the line profile whereas the strain was considered as the proportionality parameter between the Lorentzian FWHM and  $\tan\theta$  for each diffraction peak [22]. Concerning the crystallite size along the normal to the three reflection planes it may observe the largest crystallite size (i.e. between 40 and 54 nm) along the normal direction to the (220) plane and the lowest crystallite size (i.e. between 19 and

24 nm) along the normal direction to the (200) plane. To note that, the behavior of crystallite size in Fig. 5(b) is in qualitative agreement with the behavior of the crystalline texture presented in Fig. 5(a) and both support the idea of formation of ellipsoidal crystallites oriented perpendicular to the (220) reflection plane and with an aspect ratio depending on the electrodeposition potential. The behavior of strains (Fig. 5(c)) is opposite to the one of crystallite size, namely a higher strain is observed along to the normal to the (200) plane and a four times lower strain along the normal to the (220) plane. However, no significant variation of the strain with the deposition potential is to be mentioned, as indication of a rather insignificant role on the magnetic texture which is very sensitive to the deposition potential.

Expectedly, the ellipsoidal crystallite of higher aspect ratio (i.e. with a maximum value of about 3) as obtained for deposition potentials more electropositive than  $-900\,\mathrm{mV}$  will orient parallel to the nanowire length. Therefore, there will be always even for such deposition potentials, some [111] directions representing also local magnetization easy axis which will have other orientation than the cylinder axis, giving rise to the above-mentioned angular distribution of the magnetic moments at remanence or in low applied magnetic fields. To note that, with the decreasing of the deposition potential towards  $-1000\,\mathrm{mV}$ , the aspect ratio is decreasing (i.e. to a minimum value of about 2) and the crystalline texture associated to all the investigated direction becomes close to 1, meaning almost no textured polycrystalline samples. This must be also related to the lowest magnetic texture associated to sample S4.

Another possibility to characterize the magnetic texture of the samples is through the ratio  $R_{\rm C}$  between the coercive fields in parallel and perpendicular geometry, respectively. As previously discussed in case of a domain wall nucleation model, for a very high magnetic texture, a linear variation of magnetization with negligible coercive field should be obtained in perpendicular geometry and a quasi-rectangular loop of finite coercive field which increases slightly with the magnetization, in parallel geometry [1]. By decreasing the magnetic texture, the coercive field in perpendicular geometry will increase and the one in parallel geometry will decrease. That is, very high values of  $R_{\rm C}$  will characterize a high texture decreasing towards values closer to 1 (depending on the magnetization reversal model) in case of negligible magnetic texture. The evolution of the coercive fields versus temperature for all the analyzed samples is shown in Fig. 6(a) in parallel geometry and Fig. 6(b) in perpendicular geometry.

As expected, the coercive field decreases with temperature in both geometries, but in a faster manner in parallel geometry. At the lowest temperature of 5 K, where dynamical effects are suppressed, the coercive field in perpendicular geometry is linearly increasing with the decreasing of the deposition potential (from 120 Oe corresponding to sample obtained at -700 mV to 420 Oe corresponding to sample obtained at -900 mV) and then presenting a sharp increment at about 1450 Oe for sample obtained at -1000 mV. Accordingly,  $R_C$  decreases

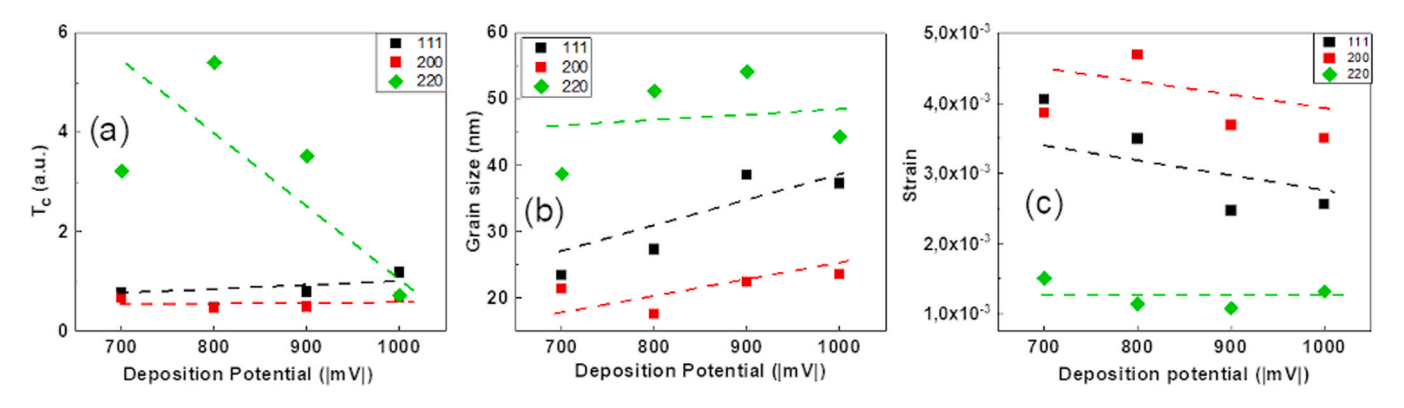
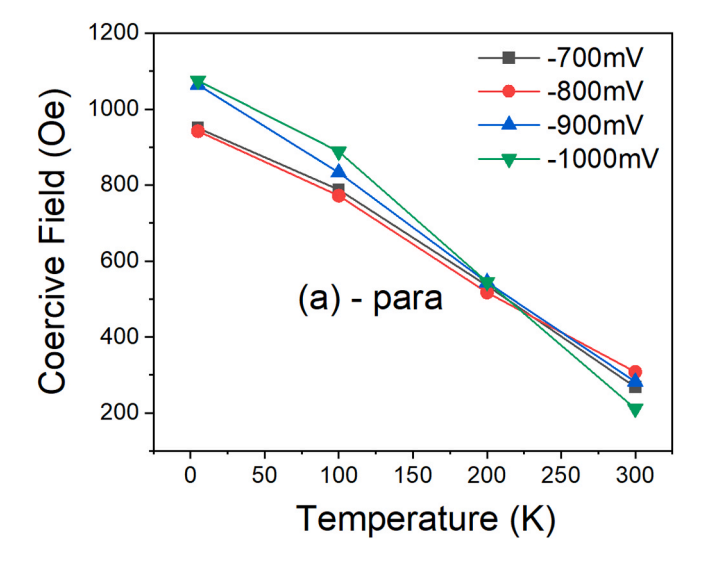
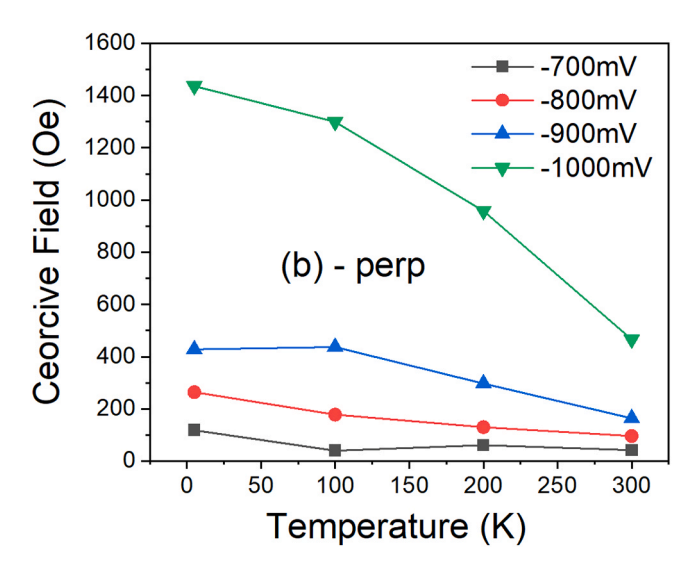


Fig. 5. Texture coefficient (a), crystallite size (b) and strain (c) along perpendicular directions to the reflection planes as estimated for samples obtained at different deposition potentials.





**Fig. 6.** Coercive fields at different temperatures for the 4 samples obtained at electrodeposition potentials between -700 and -1000 mV. The same two geometries, with the field applied parallel (a) and perpendicular (b) to the nanowires are considered.

from a value of 9 (high magnetic texture) for nanowires obtained at a deposition potential of -700 mV down to a value of 0.9 (low magnetic texture) for nanowires obtained at a deposition potential of -1000 mV.

There are 2 striking effects related to the coercive field values in parallel geometry, which seem to give support for a localized domain wall nucleation model during the magnetization reversal, initially discussed in [27]. Firstly, the values of the coercive fields are in the range from 970 to 1080 Oe, as compared to the values of a switching field specific to a Stoner-Wohlfarth applied to metallic Ni (H<sub>S</sub>=  $2\pi M_s$ ), e.g. estimated at about 3000 Oe [27]. Secondly, the coercive field is increasing by about 10 % in nanowires when the saturation magnetization decreases at half (see samples S1 and S4). This behavior is against the micromagnetic calculations performed in [25] in the frame of a delocalized domain wall nucleation model showing that the coercive field decreases by about 20 % when the saturation magnetization decreases at half. To note that at variance to the delocalized nucleation model which extend throughout the whole nanowire, the localized model of magnetization reversal suppose that the nucleation of magnetic walls starts in very small volumes of the ferromagnetic entity with inhomogeneous magnetization states. It is localized on the vicinity of structural imperfections and magnetic defects as for examples found at the grain boundaries or at the wire ends and therefore, polycrystallinity, local fluctuations in the wire diameter as well as crystalline or magnetic defects can represent cause of localization. In case of polycrystalline wires, which can be seen as random-anisotropy ferromagnets, a superposition of interacting magnetic domains of Stoner-Wohlfarth type can be considered, with the interaction depending on the ratio between the wire diameter, D, and the grain size, D<sub>0</sub>, as well as between the exchange length parameter,  $\lambda_{ex}$ , and the grain size<sup>26</sup>. If D<sub>0</sub> is higher than  $k\lambda_{ex}$ (where the product  $k\lambda_{ex}$  with k of unity order, can be interpreted as the correlation length), there are no cooperative interactions between the grains. That leads to an ordinary weak coupling regime between the grains, which can be approximated by a simple superposition of non-interacting Stoner-Wohlfarth-like magnetic grains with angular distribution of easy axis. It is to be mentioned that hysteresis loops of a superposition of Stoner-Wohlfarth-like magnetic domains with angular distribution of easy axis present a peculiar feature [29,35], namely they present a real switching field where the magnetization drops steeply (both the switching field and the drop in magnetization depending on the angular distribution of the easy axis). While for the present samples there have been not observed such drops in magnetization, the ordinary weak coupling regime should be excluded. However, according to Fig. 5 (b), the average grain size D<sub>0</sub> increases continuously from about 28 nm in sample S1 to about 36 nm in sample S4 (35 nm in sample S3), in conditions that the nanowire diameter is approximately 100 nm and  $\lambda_{ex}$ is estimated here at about 28 nm (26 nm was reported in [36]). Accordingly, the ratio D/D<sub>0</sub> decreases continuously from 3.6 in sample S1-2.8 in sample S4 (2.9 in sample S3). On the other hand, the ratio  $\lambda_{ex}/D_0$  decreases continuously from 1 in sample S1 to about 0.78 in sample S4 (0.82 in S3). Expectedly, sample S4 with no magnetic texture and lack of crystalline texture has to be characterized by a 3-dimensional Imry and Ma random anisotropy magnetic configuration [37] whereas samples S1 and S2 with enhanced magnetic texture by the cooperative quasi-1-dimensional super-spin system. Sample S3, of intermediate texture must be at the border of the two above magnetic configurations. According to the magnetic phase diagram of polycrystalline wires presented in [36], a  $\lambda_{ex}/D_0$  ratio of about 1.15 corresponds to a D/D<sub>0</sub> ratio of 2.9 as specific to sample S3 considered at the limit of the two configurations. Hence a value of 1.4 (i.e. from the ratio 1.15/0.82) is obtained for k in order to frame sample S3 at the border of the 3d Imry & Ma configuration and the quasi 1-dimensional superspin configuration in the rescaled diagram [26] (with the ordinate variable  $\lambda_{ex}/D_0$  modified to  $k\lambda_{ex}/D_0$ , where k=1.4). The product  $k\lambda_{ex}$  representing the correlation length, provides a value of about 40 nm, almost identical with the value of about 40 nm for the nucleation of a vortex wall mode in a nanowire with diameter approaching the grain size (truly 1-dimensional and cooperative system according to [26]). In fact, it is this correlation length parameter  $k\lambda_{ex}$  instead of the exchange length parameter  $\lambda_{ex}$ , to be compared with the crystallite size in order to draw physical conclusions on the cooperative interactions between the Stoner-Wohlfarth like magnetic domains associated to the crystallites. In other words, the magnetic texture is achieved or not depending on the relation between the crystallite size and the magnetic coherence length, which mainly depends on the square of the overall saturation magnetization of the wire (similar to the shape anisotropy energy of the overall wire). If the crystallite size is lower than the coherence length, more crystallites interact cooperatively leading to a magnetic texture along the anisotropy axis of the wire (e.g. as present in case of samples S1 and S2). If the crystallite size is larger than the coherence length, no cooperative interactions are possible between the crystallites and an assembly of almost independent magnetic moments of the crystallites with own local anisotropies (behaving as in a Stoner-Wohlfarth model) is achieved. To note the different sources of the local magnetic anisotropies (if the magneto-crystalline anisotropy of Ni is neglected, still is possible to have a surface related contribution [38] or shape related contributions, as in the present case of ellipsoidal crystallites with aspect ratios between 2

and 3). Considering the typical case of sample S4, with nanowires formed by crystallite with: (i) aspect ratio of 2, (ii) crystallite sizes larger than the coherence length, (iii) local shape related anisotropy and with lack of crystalline texture of nanowires meaning random orientation of the ellipsoidal crystallites, a Stoner-Wohlfarth type system with randomly oriented magnetic easy axis and hence with negligible magnetic texture is obtained.

The strong relation between the morpho-structural aspects of the polycrystalline nanowires and their magnetic properties, including their magnetic texture and magnetic reversal mechanism was also reported in [39-41]. Micromagnetic models were mainly used and the results compared with experiments on arrays of Ni (and Co) ferromagnetic nanowires grown on porous aluminum oxide with 25 nm pore diameter. Careful TEM analysis have evidenced the polycrystalline nature of the dispersed nanowires consisting of chain of successive ellipsoidal crystallites with the lateral size of about 25 nm and longitudinal size of 50 nm, e.g. approaching an aspect ratio of 2, i.e. close to the reported sizes in this work (clear TEM information on polycrystalline nanowires of 100 nm in diameter is not reliable in this respect due to the superposition of many crystallites in the front of the electron beam). The change of morphology was experimentally induced by thermal treatments, assumed to enhance the interatomic diffusion at the ellipsoid ends, leading finally to ellipsoids of increased aspect ratio, approaching better the morphology of sample S1 and S2. However, from the experimental point of view, there are 2 main differences between samples S1 and S2 and the samples grown in aluminum oxides: (i) the inter-wire distance is much higher in S1 and S2 and therefore the dipolar interactions between wires in S1 and S2 can be better neglected and (ii) the wire diameter is 4 times larger than the lateral size of the crystallite as compared to the wires grown to in aluminum oxides where the wire diameter equate the lateral size of the crystallite, assuring the 1-dimmesnional super-spin structure of the chain. However, due to the specific condition for a cooperative interaction among the crystallites in samples S1 and S2, a quasi-1-dimensional super-spin system is also expected in this case, with comparable magnetic behavior for both type of systems. Concerning the micromagnetic simulations done on arrays of nanowires consisting of chains of crystallites with lateral size of 25 nm, both ellipsoidal crystallites with aspect ratio higher than 2 as well as cuboidal crystallites were considered. The magnetization reversal loops were computed at different directions of the applied field versus the length of the nanowires. The values of the coercive fields for arrays of chains of ellipsoidal crystallites with aspect ratios higher than 2 (simulating the annealed samples at 300 C in Ar atmosphere) which reproduce well the experimental data are close to 1000 Oe in parallel geometry and about 200 Oe in perpendicular geometry [39,40]. To note that samples S1 and S2, which approach well the above-mentioned case of the 1-dimmesnional super-spin structure, show similar values for the coercive fields in both geometries. Concerning the values of  $R = M_R/M_S$ , the most reliable results to be compared with samples S1 and S2 are obtained via simulations with the largest intra-chain distance of 65 nm [40] or 70 nm [41], where the dipolar interaction between the wires is the weakest one. Accordingly, the ratio R is close to 1 in parallel geometry and close to 0 in perpendicular geometry, similar to the values reported in this work. When decreasing the aspect ratio of the crystallites, down to the case of cuboidal crystals [41], the ratio R decreases to 0.5 in longitudinal geometry, approaching better the magnetic behavior of sample S4 with its diminished crystalline texture. Finally, this picture of a polycrystalline nanowire with magnetic defects and atomic imperfections at the grain boundaries can also explain the evolution of the saturation magnetization in the considered samples. The magnetic defects and atomic imperfections at the grain boundaries lead to very distributed exchange integrals and values of the magnetic moments and hence to very distributed local anisotropies which can be transferred to the superspins of the grains, depending on the relationship between the grain size and the exchange length parameter. Tuning the dominance of the random orientation of the spins versus the 1-dimensional orientation

along the nanowire length through the deposition potential leads also to progressively lower values of the saturation magnetization of the systems.

#### 4. Conclusions

Electrodeposition in polymer ion track membranes was employed as a method to produce Ni nanowires. Since the method employs as templates membranes with uniform, high aspect ratio pores, the fabrication process leads to uniform nanowire arrays with diameter of approximately 100 nm and lengths of about 30  $\mu$ m, for all nanowires. Several values of the electrodeposition potential were employed, and it was found that this experimental parameter influences both the crystalline structure of the nanoobjects and their magnetic properties. By analyzing the experimental results according to existing models, it was found that the magnetic properties are influenced by the structural properties of the polycrystalline nanowires, including here grain size and shape and atomic imperfection/magnetic defects mainly located at the grain boundaries. Depending on the electrodeposition potential, the magnetic behavior of the obtained nanowires ranges from specific to Imry and Ma random anisotropy magnetic configurations of negligible magnetic texture to specific cooperative quasi 1-dimensional superspin configurations of much enhanced magnetic texture. The results are of utmost importance for potential applications where such arrays can be employed including spin-based information processing and storage devices. A new paradigm for controlling the magnetic anisotropy of the system through local morpho-structural aspects imposed by the processing parameters (e.g. the electrodeposition potential), in conditions of a theoretically expected highly dominant shape anisotropy in case of an usual ferromagnetic order of the Ni spins is proposed.

#### **Author contributions**

The manuscript was written through contributions of all authors. All authors have given approval to the final version of the manuscript. Melania Onea performed the preparation experiments (polycarbonate membrane etching, electrode deposition, Ni electrodeposition), performed data analysis experiments, Nicusor Iacob performed magnetic characterization and magnetic data analysis, Gabriel Schinteie performed magnetic characterization and magnetic data analysis, Maria Eugenia Toimil Molares performed membrane irradiation with swift heavy ions and was involved in data analysis and in writing the final version of the paper, Elena Matei coordinated preparation experiments, performed SEM measurements and data analysis, was involved in writing the first version and the final version of the paper, Victor Kuncser coordinated magnetic characterization experiments, performed data analysis and elaborated the magnetism discussion, was involved in writing the first version and the final version of the paper, Ionut Enculescu coordinated the work, contributed to writing the first draft and the final version of the paper.

#### CRediT authorship contribution statement

Elena Matei: Writing – review & editing, Writing – original draft, Methodology, Investigation, Formal analysis, Data curation, Conceptualization. Victor Kuncser: Writing – review & editing, Writing – original draft, Validation, Methodology, Investigation, Formal analysis, Data curation, Conceptualization. Gabriel Schinteie: Writing – review & editing, Investigation, Data curation. Maria Eugenia Toimil Molares: Writing – review & editing, Methodology, Investigation, Data curation, Conceptualization. Melania Onea: Writing – review & editing, Writing – original draft, Investigation, Data curation, Conceptualization. Nicusor Iacob: Writing – review & editing, Writing – original draft, Investigation, Data curation, Conceptualization. Enculescu Ionut-Marius: Writing – review & editing, Writing – original draft, Methodology, Investigation, Formal analysis, Data curation, Conceptualization.

#### **Funding**

The authors acknowledge the financial contribution of the Romanian Ministry of Research, Innovation and Digitalization through PNRR-funded project no. 766083/23.05.2023, and through Nucleu programme PC1-PN23080101.

#### **Declaration of Competing Interest**

The authors declare that they have no known competing financial interests or personal relationships that could have appeared to influence the work reported in this paper.

#### References

- A. Costas, C. Florica, E. Matei, M.E. Toimil-Molares, I. Stavarache, A. Kuncser, V. Kuncser, I. Enculescu, Magnetism and magnetoresistance of single Ni–Cu alloy nanowires, Beilstein J. Nanotechnol. 9 (2018) 2345–2355, https://doi.org/ 10.3762/binano.9.219.
- [2] E. Matei, I. Enculescu, M.E. Toimil-Molares, A. Leca, C. Ghica, V. Kuncser, Magnetic configurations of Ni–Cu alloy nanowires obtained by the template method, J. Nanopart. Res. 15 (2013) 1863, https://doi.org/10.1007/s11051-013-1863.3
- [3] A. Fernández-Pacheco, L. Serrano-Ramón, J.M. Michalik, M.R. Ibarra, J.M. De Teresa, L. O'Brien, D. Petit, J. Lee, R.P. Cowburn, Three dimensional magnetic nanowires grown by focused electron-beam induced deposition, Sci. Rep. 3 (2013) 1492, https://doi.org/10.1038/srep01492.
- [4] S. Kim, H. Yoon, H. Lee, S. Lee, Y. Jo, S. Lee, J. Choo, B. Kim, Epitaxy-driven vertical growth of single-crystalline cobalt nanowire arrays by chemical vapor deposition, J. Mater. Chem. C. Mater. 3 (2015) 100–106, https://doi.org/10.1039/ CATCO17651
- [5] A.M. Toufiq, F. Wang, Q. Javed, Q. Li, Y. Li, Hydrothermal synthesis of MnO2 nanowires: structural characterizations, optical and magnetic properties, Appl. Phys. A 116 (2014) 1127–1132, https://doi.org/10.1007/s00339-013-8195-0.
- [6] F. Elhoussine, S. Mátéfi-Tempfli, A. Encinas, L. Piraux, Conductance quantization in magnetic nanowires electrodeposited in nanopores, Appl. Phys. Lett. 81 (2002) 1681–1683, https://doi.org/10.1063/1.1503400.
- [7] R. Ferré, K. Ounadjela, J.M. George, L. Piraux, S. Dubois, Magnetization processes in nickel and cobalt electrodeposited nanowires, Phys. Rev. B 56 (1997) 14066–14075, https://doi.org/10.1103/PhysRevB.56.14066.
- [8] C. Florica, E. Matei, A. Costas, M.E.T. Molares, I. Enculescu, Field effect transistor with electrodeposited ZnO nanowire channel, Electro Acta 137 (2014) 290–297, https://doi.org/10.1016/j.electacta.2014.05.124.
- [9] E. Matei, C. Florica, A. Costas, M.E. Toimil-Molares, I. Enculescu, Electrical properties of single CdTe nanowires, Beilstein J. Nanotechnol. 6 (2015) 444–450, https://doi.org/10.3762/bjnano.6.45.
- [10] E. Matei, A. Costas, C. Florica, M. Enculescu, I. Pintilie, L. Pintilie, I. Enculescu, Electrical properties of templateless electrodeposited ZnO nanowires, Mater. Sci. Semicond. Process 42 (2016) 364–372, https://doi.org/10.1016/j.
- [11] A. Fert, L. Piraux, Magnetic nanowires, J. Magn. Magn. Mater. 200 (1999) 338–358, https://doi.org/10.1016/S0304-8853(99)00375-3.
- [12] S. Kumar, S.K. Chakarvarti, Large-scale synthesis of uniform nickel nanowires and their characterisation, J. Exp. Nanosci. 5 (2010) 126–133, https://doi.org/ 10.1080/17458080903314048.
- [13] C. Scho, B.M.I. Van Der Zande, L.G.J. Fokkink, M. Henny, C. Schmid, M. Kru, A. Bachtold, R. Huber, H. Birk, U. StauferTemplate Synthesis of Nanowires in Porous Polycarbonate Membranes: Electrochemistry and Morphology, 1997. https://pubs.acs.org/sharingguidelines.
- [14] J.L. Cardoso, G. Gozzi, S.G. Dos Santos Filho, Fabrication and physical characterization of nickel nanowires formed by a Template-Based electrodeposition method, ECS Trans. 14 (2008) 457–466, https://doi.org/ 10.1149/1.2955061.
- [15] Y.H. Chen, J.L. Duan, H.J. Yao, D. Mo, T.Q. Liu, T.S. Wang, M.D. Hou, Y.M. Sun, J. Liu, Facile preparation and magnetic properties of ni nanotubes in polycarbonate ion-track templates, Phys. B Condens Matter 441 (2014) 1–5, https://doi.org/ 10.1016/j.physb.2014.02.002.
- [16] A. Sugawara, D. Streblechenko, M. McCartney, M.R. Scheinfein, Magnetic coupling in self-organized narrow-spaced fe nanowire arrays, IEEE Trans. Magn. 34 (1998) 1081–1083, https://doi.org/10.1109/20.706363.
- [17] F. Muench, S. Schaefer, M. Méndez, J.A. Fernández-Roldán, A.S. González-García, V. Vega, U. Kunz, W. Ensinger, J. García, V.M. Prida, Magneto-structural properties of rhombohedral ni and Ni-B nanotubes deposited by electroless-plating in track-

- etched mica templates, J. Mater. Chem. C. Mater. 11 (2023) 9271–9280, https://doi.org/10.1039/d3tc00857f.
- [18] M. Vázquez, K. Pirota, M. Hernández-Vélez, V.M. Prida, D. Navas, R. Sanz, F. Batallán, J. Velázquez, Magnetic properties of densely packed arrays of ni nanowires as a function of their diameter and lattice parameter, J. Appl. Phys. (2004) 6642–6644, https://doi.org/10.1063/1.1687539.
- [19] A.Kazadi Mukenga Bantu, J. Rivas, G. Zaragoza, M.A. López-Quintela, M.C. Blanco, Structure and magnetic properties of electrodeposited cobalt nanowires, J. Appl. Phys. 89 (2001) 3393–3397, https://doi.org/10.1063/1.1345857.
- [20] E.M. Palmero, M. Méndez, S. González, C. Bran, V. Vega, M. Vázquez, V.M. Prida, Stepwise magnetization reversal of geometrically tuned in diameter ni and FeCo bisegmented nanowire arrays, Nano Res. 12 (2019) 1547–1553, https://doi.org/ 10.1007/s12274-019-2385-9.
- [21] J. Gao, W. Jie, Y. Yuan, T. Wang, G. Zha, J. Tong, Dependence of film texture on substrate and growth conditions for CdTe films deposited by close-spaced sublimation, J. Vacuum Sci. Technol. A Vacuum Surfaces Films 29 (2011), https:// doi.org/10.1116/1.3610177.
- [22] C. Suryanarayana, M.G. Norton, X-Ray diffraction, Springer US, Boston, MA, 1998, https://doi.org/10.1007/978-1-4899-0148-4.
- [23] J. He, Q. Zhang, An exact calculation of the voigt spectral line profile in spectroscopy, J. Opt. A Pure Appl. Opt. 9 (2007) 565–568, https://doi.org/ 10.1088/1464-4258/9/7/003.
- [24] K.J. Klabunde, Nanoscale materials in chemistry, Wiley, 2001, https://doi.org/ 10.1002/0471220620.
- [25] P. Stamenov, J.M.D. Coey, Sample size, position, and structure effects on magnetization measurements using second-order gradiometer pickup coils, Rev. Sci. Instrum. 77 (2006) 1–11, https://doi.org/10.1063/1.2149190.
- [26] M. Sawicki, W. Stefanowicz, A. Ney, Sensitive SQUID magnetometry for studying nanomagnetism, Semicond. Sci. Technol. 26 (2011) 064006, https://doi.org/ 10.1088/0268-1242/26/6/064006.
- [27] D.J. Sellmyer, M. Zheng, R. Skomski, Magnetism of fe, co and ni nanowires in self-assembled arrays, J. Phys. Condens. Matter 13 (2001) R433–R460, https://doi.org/10.1088/0953-8984/13/25/201.
- [28] C.A. Ross, M. Hwang, M. Shima, J.Y. Cheng, M. Farhoud, T.A. Savas, H.I. Smith, W. Schwarzacher, F.M. Ross, M. Redjdal, F.B. Humphrey, Micromagnetic behavior of electrodeposited cylinder arrays, Phys. Rev. B 65 (2002) 144417, https://doi. org/10.1103/PhysRevB.65.144417.
- [29] A. Kuncser, V. Kuncser, Magnetization reversal via a Stoner–Wohlfarth model with bi-dimensional angular distribution of easy axis, J. Magn. Magn. Mater. 395 (2015) 34–40, https://doi.org/10.1016/j.jmmm.2015.07.035.
- [30] M. Beleggia, S. Tandon, Y. Zhu, M. De Graef, On the magnetostatic interactions between nanoparticles of arbitrary shape, J. Magn. Magn. Mater. 278 (2004) 270–284, https://doi.org/10.1016/j.jmmm.2003.12.1314.
- [31] R. Richter, H. Eschrig, LCAO-CPA for disordered ferromagnetic 3d transition metal alloys. Magnetic moment formation in NiCu and FeCo, Phys. Scr. 37 (1988) 948–951, https://doi.org/10.1088/0031-8949/37/6/022.
- [32] L. Sun, Y. Hao, C.-L. Chien, P.C. Searson, Tuning the properties of magnetic nanowires, IBM J. Res Dev. 49 (2005) 79–102, https://doi.org/10.1147/ rd.491.0079.
- [33] N. Han, G. Guo, L. Zhang, G. Zhang, W. Song, Magnetization reversal for ni nanowires studied by micromagnetic simulations, J. Mater. Sci. Technol. 25 (2009) 151–154.
- [34] A. Kuncser, S. Antohe, V. Kuncser, A general perspective on the magnetization reversal in cylindrical soft magnetic nanowires with dominant shape anisotropy, J. Magn. Magn. Mater. 423 (2017) 34–38, https://doi.org/10.1016/j. immm.2016.09.066.
- [35] V. Kuncser, P. Palade, A. Kuncser, S. Greculeasa, G. Schinteie, Engineering Magnetic Properties of Nanostructures via Size Effects and Interphase Interactions, in: 2014: pp. 169–237. https://doi.org/10.1007/978-3-662-44479-5\_7.
- [36] R. Skomski, H. Zeng, M. Zheng, D.J. Sellmyer, Magnetic localization in transition-metal nanowires, Phys. Rev. B 62 (2000) 3900–3904, https://doi.org/10.1103/PhysRevB.62.3900.
- [37] Y. Imry, S. Ma, Random-Field instability of the ordered state of continuous symmetry, Phys. Rev. Lett. 35 (1975) 1399–1401, https://doi.org/10.1103/ PhysRevLett.35.1399.
- [38] J. Holanda, C.L.A.V. Campos, C.A. Franca, E. Padrón-Hernández, Effective surface anisotropy in polycrystalline ferromagnetic nanowires, J. Alloy. Compd. 617 (2014) 639–641, https://doi.org/10.1016/j.jallcom.2014.07.219.
- [39] J. Holanda, D.B.O. Silva, E. Padrón-Hernández, Angular dependence of the coercivity in arrays of ferromagnetic nanowires, J. Magn. Magn. Mater. 378 (2015) 228–231, https://doi.org/10.1016/j.jmmm.2014.11.046.
- [40] G.P. Fuentes, J. Holanda, Y. Guerra, D.B.O. Silva, B.V.M. Farias, E. Padrón-Hernández, Micromagnetic simulation and the angular dependence of coercivity and remanence for array of polycrystalline nickel nanowires, J. Magn. Magn. Mater. 423 (2017) 262–266, https://doi.org/10.1016/j.jmmm.2016.09.107.
- [41] Y. Guerra, R. Peña-Garcia, E. Padrón-Hernández, Magnetic reversion in real nickel and cobalt nanowires and the angular dependence of coercivity, J. Magn. Magn. Mater. 452 (2018) 17–22, https://doi.org/10.1016/j.jmmm.2017.12.030.